

$\chi^{(5)}$  susceptibility stabilizes the propagation of ultrashort laser pulses in air

Antoine Vinçotte and Luc Bergé

*Département de Physique Théorique et Appliquée, CEA/DAM Ile de France, Boîte Postale 12, 91680 Bruyères-le-Châtel, France*

(Received 16 July 2004; published 13 December 2004)

The influence of higher-order optical nonlinearities on the self-guiding of femtosecond pulses in the atmosphere is investigated theoretically.  $\chi^{(5)}$  susceptibility, even small, is shown to significantly affect the propagation dynamics and enhance the robustness of femtosecond filaments by lowering the threshold intensity at which the beam saturates and by enlarging the self-channeling range.

DOI: 10.1103/PhysRevA.70.061802

PACS number(s): 42.65.Jx, 42.65.Re, 42.68.Ay

Femtosecond laser pulses are known to produce intense channels of light in the atmosphere [1], which result from the competition between the Kerr focusing of the beam and self-induced ionization of air molecules. These channels consist of filamentary structures with  $\sim 1$  mJ energy, 100  $\mu\text{m}$  waist, peak intensities attaining  $10^{13}$ – $10^{14}$  W/cm<sup>2</sup>, and generating an electron plasma with densities around  $10^{16}$  cm<sup>-3</sup> [2,3].

So far, attention has mostly been paid to the previous interplay, where only plasma generation arrests the beam collapse. Several authors, however, proposed other stabilizers for this saturation process. For instance, chromatic dispersion was recently shown to promote a self-guiding with no major role from ionization in condensed media such as water [4]. Nonetheless, this property does not usually hold in air, for which the dispersion is so weak that it cannot stop the collapse of high-power beams before plasma occurs. Instead,  $\chi^{(5)}$  contributions originating from the expansion of the nonlinear polarization vector may arise in the atmosphere at intensity levels close to the ionization threshold. Therefore, they appear as potential key players in the self-channeling mechanism. In Refs. [5,6],  $\chi^{(5)}$  defocusing nonlinearities were shown to affect both the saturation intensity of self-guided filaments and their associated peak electron densities. In contrast, a recent investigation [7] proposed that quintic saturation should be omitted in current models, as ionization processes dominate with an intensity threshold below that of the  $\chi^{(5)}$  effects. Here, comparisons were performed from intensity thresholds considered independently of each other. The analysis, moreover, applied to a reduced model ignoring the role of the Raman-delayed Kerr response in air and multiphoton absorption. Thus, the question of knowing whether and why  $\chi^{(5)}$  nonlinearities are important in the self-channeling of ultrashort light pulses still remains open.

In this paper, we provide theoretical arguments displaying evidence of the importance of such terms in the pulse dynamics, even when they exhibit a small  $\chi^{(5)}$  coefficient. We show that a combination of both  $\chi^{(5)}$  and free electron excitation makes a quintic susceptibility have noticeable influence on the filamentation process and enlarges the self-guiding range. A two-scale variational approach supports these theoretical expectations. Numerical simulations of radially symmetric and fully (3D+1)-dimensional pulses clearly demonstrate this property.

To start with, we consider the propagation equations for the slowly varying envelope  $\mathcal{E}(x, y, t, z)$  of the beam evolving along the  $z$  axis, written as [8,9]

$$\frac{\partial \mathcal{E}}{\partial z} = \frac{i}{2k_0} \nabla_{\perp}^2 \mathcal{E} - i \frac{k''}{2} \partial_t^2 \mathcal{E} + ik_0 \frac{\Delta n}{n_0} \mathcal{E} - \frac{\beta(|\mathcal{E}|^2)}{2} \mathcal{E} - \frac{\sigma}{2} \rho \mathcal{E}, \quad (1)$$

$$\frac{\Delta n}{n_0} \equiv n_2 R(t) - n_4 |\mathcal{E}|^4 - \frac{\rho}{2\rho_c}, \quad (2)$$

$$R(t) \equiv (1 - \theta) |\mathcal{E}(t)|^2 + \frac{\theta}{\tau_K} \int_{-\infty}^t e^{-(t-t')/\tau_K} |\mathcal{E}(t')|^2 dt', \quad (3)$$

$$\partial_t \rho = W(|\mathcal{E}|^2) \rho_{\text{nt}} + \frac{\sigma}{U_i} \rho |\mathcal{E}|^2. \quad (4)$$

These equations apply to femtosecond pulses moving in their group-velocity frame, with the central wave number  $k_0 = 2\pi/\lambda_0$  and  $\nabla_{\perp}^2 \equiv \partial_x^2 + \partial_y^2$ . We consider the laser wavelength  $\lambda_0 = 800$  nm, normal group-velocity dispersion with coefficient  $k'' = 0.2$  fs<sup>2</sup>/cm, and a critical plasma density  $\rho_c = 1.8 \times 10^{21}$  cm<sup>-3</sup>. Only ionization of dioxygen molecules is considered, with the gap potential  $U_i = 12.1$  eV and an initial neutral density  $\rho_{\text{nt}} = 5.4 \times 10^{18}$  cm<sup>-3</sup>. The last terms in Eq. (1) are related to multiphoton absorption (MPA) expressed as  $\beta(|\mathcal{E}|^2) \equiv \rho_{\text{nt}} W(|\mathcal{E}|^2) U_i / |\mathcal{E}|^2$  and to avalanche ionization with a cross section for inverse bremsstrahlung  $\sigma = 5.44 \times 10^{-20}$  cm<sup>2</sup>, respectively. In Eq. (2),  $\Delta n/n_0$  is the effective optical index ( $n_0 = 1$ ). It describes the competition between the instantaneous and Raman-delayed Kerr responses of air in ratio  $\theta$  ( $\tau_K = 70$  fs,  $n_2 = 4 \times 10^{-19}$  cm<sup>2</sup>/W), the quintic saturation with coefficient  $n_4 \sim |\chi^{(5)}|$ , and plasma generation. The critical power for self-focusing is  $P_{\text{cr}} = \lambda_0^2 / 2\pi n_2 = 2.55$  GW. As no precise value for  $n_4$  is nowadays available for dioxygen molecules, we adopt the same reasoning as in Ref. [6]: For noble gases with ionization potential close to oxygen,  $\chi^{(5)}$  is expected to scale as  $\chi^{(5)} \sim 10^{-29}$ – $10^{-28}$  (esu), leading to  $n_4$  contained in the interval  $10^{-33}$ – $10^{-32}$  cm<sup>4</sup>/W<sup>2</sup>. Therefore, two different reasonable estimates will be tested here, namely,  $n_4 = 10^{-32}$  cm<sup>4</sup>/W<sup>2</sup> and  $n_4 = 2.5 \times 10^{-33}$  cm<sup>4</sup>/W<sup>2</sup>.

Equation (4) describes the evolution of the plasma density  $\rho$ , whose ionization rate  $W(I)$  with  $I \equiv |\mathcal{E}|^2$  follows the so-called PPT model proposed by Perelomov *et al.* in [10]. At moderate intensities  $I \leq 5 \times 10^{13}$  W/cm<sup>2</sup>,  $W(I)$  recovers the multiphoton ionization (MPI) rates  $W(I) = \sigma_{(K)} I^K$ , where  $K$  is the number of photons required for ionization. At higher intensities, tunnel ionization dominates, and the functional de-

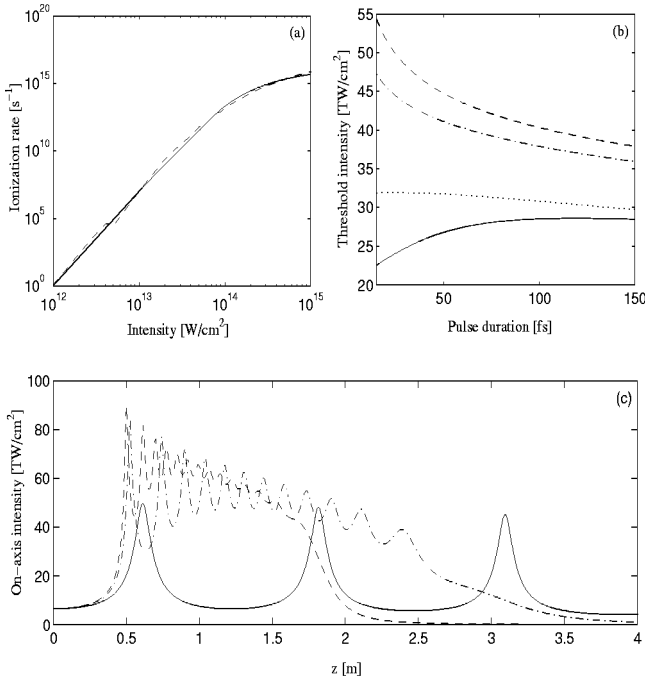


FIG. 1. (a) Ionization rates  $W(I)$  vs laser intensity following the PPT model [10] (dashed curve) and the fitting function Eq. (5) (solid curve). (b) Threshold intensities,  $I_{\text{th}}$ , realizing  $\Delta n/n_0=0$  when  $n_4=0$  (dashed curve),  $n_4=2.5 \times 10^{-33} \text{ cm}^4/\text{W}^2$  (dash-dotted curve), and  $n_4=10^{-32} \text{ cm}^4/\text{W}^2$  for  $\theta=0.5$  (solid curve) and  $\theta=0.2$  (dotted curve). (c) On-axis intensity ( $\xi=\eta=0$ ) computed from the two-scale variational approach in the same configurations.

dependencies of  $W(I)$  depart from the MPI expression. The complete curve  $W(I)$  has been plotted in Fig. 1(a) with a dashed line. This will be used in the coming radial and 3D numerical simulations. For further convenience, it can be approximated by the fitting function represented with a solid line:

$$\log_{10}(W) = a_{1,2}[\log_{10}(I)]^{b_{1,2}} + c_{1,2}, \quad (5)$$

where the twofold constants  $a_{1,2}$ ,  $b_{1,2}$ , and  $c_{1,2}$ , differing from one another on either side of  $I \approx 6 \times 10^{13} \text{ W}/\text{cm}^2$ , have been evaluated to reproduce the PPT rate.

Below, we emphasize that even weak  $\chi^{(5)}$  contributions can be responsible for significant changes in the filament dynamics. To prove this assertion, let us compute the intensity for which  $\Delta n/n_0=0$  and compare it when the  $\chi^{(5)}$  nonlinearity is discarded or not. To estimate  $\Delta n/n_0$ , we first model the pulse by a Gaussian temporal profile  $\mathcal{E} = \sqrt{I_0} e^{-t^2/t_p^2}$  with half-width duration  $t_p$ . By plugging  $|\mathcal{E}|^2$  into Eq. (2), we find that the intensity thresholds (noted  $I_{\text{th}}$ ), at which a self-guided filament can be realized, follow from the roots of the relation

$$AI - \frac{\rho_{\text{nl}} t_p}{2\rho c n_2} W(I) - BI^2 = 0, \quad (6)$$

where the density  $\rho$  is approximated by  $\rho \approx t_p W(I) \rho_{\text{nl}}$  with  $W(I)$  given by Eq. (5).  $A \equiv \max_t R(t)$  yields the maximum Kerr response reached at the instant  $t=t_{\text{max}}$ , while  $B$

$= (n_4/n_2) e^{-4t_{\text{max}}^2}$  measures the weight of  $\chi^{(5)}$  over  $\chi^{(3)}$  susceptibilities stated at the same time.

Figure 1(b) shows the solutions of Eq. (6) involving three values of  $n_4$  versus the pulse duration  $t_p$  for  $\theta=1/2$  [8,9]. Even weak,  $\chi^{(5)}$  significantly decreases the threshold intensity  $I_{\text{th}}$ , at which the pulse starts to saturate. Consequently, ionization is not the only effect that contributes to the equilibrium resulting into a self-guided filament. This decrease is more pronounced when  $n_4$  is strong, but it becomes more attenuated at large values of  $t_p$ . The effective Kerr response determined by  $A$  increases with  $t_p$ . When plasma generation dominates (weak  $n_4$ ),  $I_{\text{th}}$  decreases with  $t_p$ . In the opposite case (strong  $n_4$ ),  $I_{\text{th}}$  increases. In both situations, however, quintic saturation participates in diminishing the overall intensity threshold. Hence, energy losses caused by MPA should be weaker and preserve the filament over longer distances.

It is also important to underline the role played by the ratio  $\theta$  in the delayed Kerr response [Eq. (3)]. A weaker value of  $\theta$  indeed increases the weight of the instantaneous cubic nonlinearity and the intensity threshold is augmented in turn [dotted curve in Fig. 1(b)].

To proceed further, we use a two-scale variational approach solving Eq. (1) and elaborated on the procedure exposed in [11] (see also [12]). The pulse dynamics is described by transverse  $[R(z)]$  and temporal  $[T(z)]$  lengths depending both on the propagation distance  $z$ . The wave envelope is modeled by the Gaussian test function:

$$\mathcal{E} = \frac{\sqrt{J(z)}}{R(z)\sqrt{T(z)}} \phi(\xi, \eta) e^{iR_z(z)R(z)\xi^2/4 - iT_z(z)T(z)\eta^2/4\delta}, \quad (7)$$

where  $\phi = e^{-\xi^2/2 - \eta^2/2}$ ,  $\xi \equiv \sqrt{x^2 + y^2}/R(z)$ ,  $\eta \equiv t/T(z)$ , and  $\delta = 2\pi n_0 w_0^2 k''/\lambda_0 t_p^2$ . Here, the sizes  $R(z)$  and  $T(z)$  have been normalized with respect to the input beam waist  $w_0$  and duration  $t_p$ , while  $J(z)$  measures the loss of power induced by MPA. For technical convenience,  $W(I)$  is simplified by considering the MPI formulation  $W(I) \approx \sigma_{(K)} I^K$  with  $K=8$  and  $\sigma_{(8)} \approx 2.9 \times 10^{-99} \text{ s}^{-1} \text{ cm}^{16}/\text{W}^8$ , which is close to Eq. (5) for  $I \approx 10^{13} - 10^{14} \text{ W}/\text{cm}^2$  [8]. Plugging the ansatz (7) into virial identities provides a set of differential equations in the form  $R_{zz} = F_R + \chi_5 J^2 p^2/R^5 T^2$ ,  $T_{zz} = F_T - \delta \chi_5 J^2 p^2/R^4 T^3$ ,  $J_z = F_J$ , where  $p \equiv P_{\text{in}}/P_{\text{cr}}$  is the ratio of input power over critical and  $\chi_5 \equiv 16n_4 P_{\text{cr}}/(9\sqrt{3}n_2 \pi w_0^2)$  accounts for the quintic saturation. The quantities  $F_R$ ,  $F_T$ , and  $F_J$  denote cumbersome functions depending on  $(R, T, J)$ , which can be found already established in [11,12].

Figure 1(c) illustrates the normalized on-axis intensity integrated from this variational method with  $p=10$ ,  $\theta=1/2$ , for the values of  $n_4$  selected in Fig. 1(b). The parameters for the laser pulse are  $t_p=42 \text{ fs}$  ( $A=0.66$ ),  $w_0=0.5 \text{ mm}$  and enter the input Gaussian profile  $\mathcal{E}(r, t, 0) = \sqrt{2P_{\text{in}}/\pi w_0^2} \exp(-r^2/w_0^2 - t^2/t_p^2)$ . We observe that the larger  $n_4$ , the lower the peak intensity. The typical ratio of peak intensities between the two extreme cases is 1.8, in agreement with Fig. 1(b).  $\chi^{(5)}$  saturation promotes a longer self-guiding length, along which oscillations develop with increasing  $n_4$ , until the beam

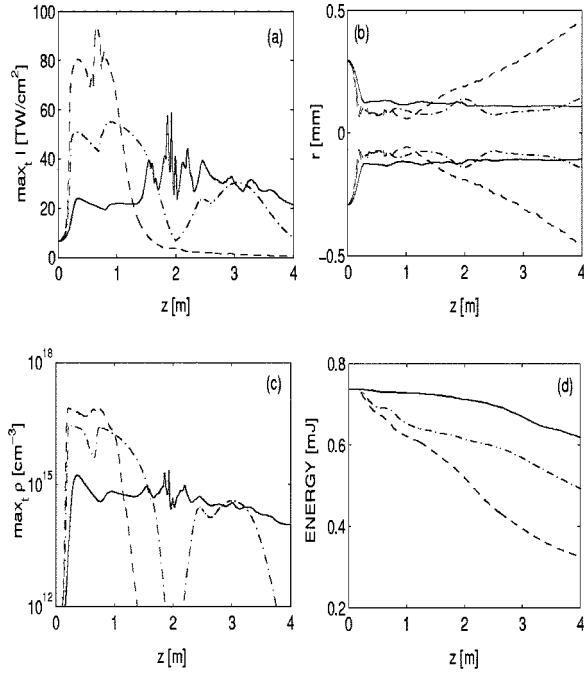


FIG. 2. (a) Peak intensity, (b) mean radius of the fluence distribution  $\mathcal{F} \equiv \int_{-\infty}^{+\infty} |\mathcal{E}|^2 dt$ , (c) peak electron density, and (d) energy losses for a 42 fs, 0.5-mm-waisted pulse undergoing plasma defocusing alone (dashed curves), plasma defocusing and  $\chi^{(5)}$  saturation with weak  $n_4$  (dash-dotted curves), and plasma and  $\chi^{(5)}$  saturation with strong  $n_4$  (solid curves).

behaves like a bright soliton in an optically saturated Kerr medium [14]. As the peak intensity decreases under the influence of  $\chi^{(5)}$ , the filament length increases.

For comparison we numerically solve Eqs. (1)–(4) using a parallel radial code ( $\nabla_{\perp}^2 \equiv r^{-1} \partial_r r \partial_r$ ,  $r = \sqrt{x^2 + y^2}$ ) for the same initial Gaussian pulse as above. Figure 2 shows that  $\chi^{(5)}$  decreases the saturation intensity and enhances the self-guiding over longer distances. This effect is reinforced when  $n_4$  is stronger, so that the  $\chi^{(5)}$  nonlinearities promote a longer and stabler propagation. By increasing the values of  $n_4$ , the peak intensity,  $I_{\text{peak}} > I_{\text{th}}$ , decreases more and more on the average, in agreement with Fig. 1(b). This has a direct consequence on the self-guiding length dictated by MPA,  $\Delta z \sim 2/\beta^{(K)} I_{\text{th}}^{K-1}$  [Fig. 3(b)], which becomes enlarged by the order of magnitude  $(I_{\text{th}}^{n_4 \neq 0}/I_{\text{th}}^{n_4=0})^{1-K}$  where the values of  $I_{\text{th}}$  can be estimated from Fig. 1(b). Moreover, the peak electron density diminishes in turn, as can be seen from Fig. 2(c). However,  $\chi^{(5)}$  saturation does not prevent plasma generation with electron densities exceeding  $10^{15} - 10^{16} \text{ cm}^{-3}$ . Lowering  $I_{\text{th}}$  also decreases the energy losses in proportion [Fig. 2(d)] and justifies the robustness of the light filament when  $n_4 \neq 0$ . Note the *qualitative* agreement between Figs. 1(c) and 2(a): The variational approach predicts intensity growths and self-channeling ranges comparable with the numerical simulations, even if this method cannot reproduce the pulse dynamics in detail (variational models based on Eq. (7) capture the overall beam power and are unable to describe, e.g., radiation of energy to the boundaries [11]). In particular, as  $n_4$  is increased to  $10^{-32} \text{ cm}^4/\text{W}^2$ , a soliton regime characterized by quasiperiodic oscillations takes place.

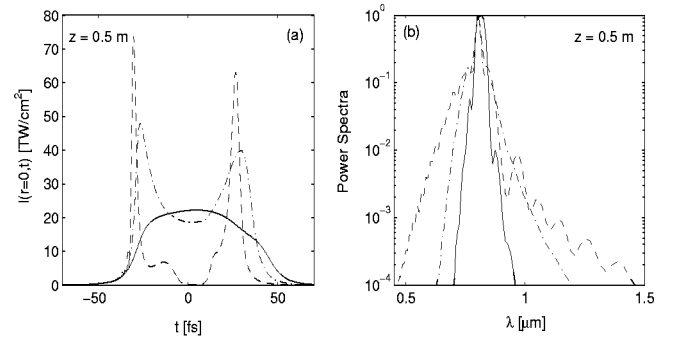


FIG. 3. (a) Temporal profiles and (b) power spectra at  $z = 0.5 \text{ m}$  for the pulses shown in Fig. 2, using the same plot style convention for the different values of  $n_4$ .

Figure 3(a) details the temporal profiles at  $z=0.5 \text{ m}$ , where the pulse is close to its maximum intensity. With no quintic saturation ( $n_4=0$ ), the back of the pulse is depleted by plasma defocusing. A sharp leading edge first survives, before plasma turns off and makes a trailing edge refocus following the scenario of Ref. [3]. This dynamics induces an asymmetry in the spectrum plotted from the Fourier transform in time of the laser intensity [Fig. 3(b)]. As  $n_4$  departs from zero, the temporal profile, however, becomes more symmetric and less intense. Thus, the pulse spectrum, whose frequency variations are governed by the ratio of the peak intensity over the pulse duration [13], exhibits broadenings of lesser extent and becomes more symmetric as  $\chi^{(5)}$  increases.

To end the present investigation, we find it instructive to display fluence distributions computed from a realistic input beam, as currently used in experiments. The goal of these computations is not to identify a proper value of the  $\chi^{(5)}$  susceptibility in air, but, instead, to underline its potential role in the multiple filamentation patterns developed by ultrashort pulses. In Refs. [2,8], femtosecond beams were shown to form a ringlike structure at  $z=2.5 \text{ m}$ . This ring became modulationally unstable and decayed into two small-scale spots self-focusing over 2–4 m. The couple of spots finally coalesced into a central lobe at  $z=8.5 \text{ m}$ . Before this distance, no plasma excitation was detected. In spite of this, the two spots remained robust upon at least 2 m before fusing. Beam parameters were  $w_0=3 \text{ mm}$ ,  $t_p=42 \text{ fs}$ , and  $P_{\text{in}}=28P_{\text{cr}}$ . To reproduce these data, we used a 3D parallel spectral code [9] solving Eqs. (1)–(4) with the previous parameters. The initial condition, chosen closely to the experimental beam, was perturbed by a 10% amplitude random noise:  $\mathcal{E}(z=0) = \sqrt{I_0} \exp\{-([x^2 + 2y^2]/w_0^2)^{3/2} - t^2/t_p^2\} [1 + 0.1 \times (\text{noise})]$ , with  $I_0 \approx 0.7 \text{ TW/cm}^2$ .

Figures 4(a)–4(c) show the fluence distribution of the pulse at increasing propagation distances (from left to right) when  $n_4=0$ . At  $z=3.7 \text{ m}$ , two spots resulting from the modulational instability of the input beam self-focus [Fig. 4(a)]. At  $z=5.1 \text{ m}$ , these filaments break up into six or seven cells, i.e., the two-spot pattern ceases to be robust [Fig. 4(b)]. At  $z=6.5 \text{ m}$ , fusion occurs (discrepancy with the experimental fusion point,  $z=8.5 \text{ m}$ , is attributed to the uncertainty in the measured input waist and in the temporal and transverse structure of the initial pulse) and the central lobe becomes

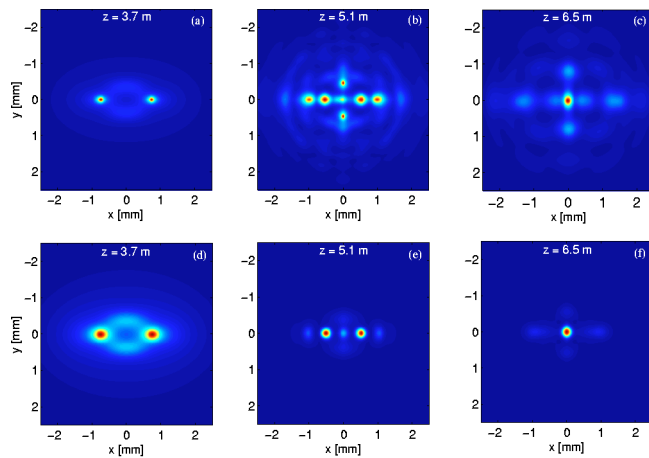


FIG. 4. (Color online) Fluence distribution of a 42 fs pulse with a 3-mm-waist computed at different propagation distances for (a)–(c)  $n_4=0$  and (d)–(f)  $n_4=10^{-32} \text{ cm}^4/\text{W}^2$ .

unstable at further distances. Maximum plasma density ( $>5 \times 10^{16} \text{ cm}^{-3}$ ) takes place as soon as  $z \geq 3.7 \text{ m}$ . Figures 4(d)–4(f) show the same pieces of information when  $n_4 = 10^{-32} \text{ cm}^4/\text{W}^2$ . Two broader cells continue to self-focus at  $z=3.7 \text{ m}$  [Fig. 4(d)]. They keep a robust state at  $z=5.1 \text{ m}$  [Fig. 4(e)] before fusing at  $z=6.5 \text{ m}$  into one filament [Fig. 4(f)], which holds its shape along several meters. In this case, maximum plasma density ( $>10^{15} \text{ cm}^{-3}$ ) arises from  $z$

$=6.2 \text{ m}$ . It stays clamped at levels less than  $10^{14} \text{ cm}^{-3}$  (i.e., below the electron detection threshold of [2]) during the preceding stages. Note that these simulations do not plead in favor of  $n_4$  as high as  $10^{-32} \text{ cm}^4/\text{W}^2$ . They, nevertheless, strongly indicate that a  $\chi^{(5)}$  response of air should not be omitted in current modelings. It is interesting to notice that, without higher-order saturation, the number of filaments formed in optical regime should be close to  $P_{\text{in}}/P_{\text{fil}} \approx 7$  with a power per filament evaluated by  $P_{\text{fil}} \approx \pi^2 P_{\text{cr}}/4A$  [14]. With a quintic saturation, this number decreases by the factor  $(1 - 2n_4 I_{\text{max}}^{\text{optic}}/An_2)$ , where  $I_{\text{max}}^{\text{optic}} \leq 10 \text{ TW}/\text{cm}^2$  denotes the maximal intensity reached without plasma formation, which suits better the experimental observations.

In conclusion, we have shown the stabilizing role of  $\chi^{(5)}$  defocusing nonlinearities in the meter-range propagation of ultrashort pulses in air. Although the precise value of  $\chi^{(5)}$  susceptibility for dioxygen molecules remains unknown, its influence should not be ignored.  $\chi^{(5)}$  saturation does not prevent plasma generation, although the latter occurs with weaker density levels. It lowers the maximum light intensity from which self-channeling develops and stabilizes femto-second filaments by enlarging significantly their self-guiding range.

The authors thank S. Skupin for technical advices on the numerical simulations and Dr. R. Nuter for providing them with the PPT ionization rate used in this work.

- 
- [1] A. Braun *et al.*, *Opt. Lett.* **20**, 73 (1995); E. T. J. Nibbering *et al.*, *ibid.* **21**, 62 (1996); B. LaFontaine *et al.*, *Phys. Plasmas* **6**, 1615 (1999).  
 [2] S. Tzortzakis *et al.*, *Phys. Rev. Lett.* **86**, 5470 (2001).  
 [3] M. Mlejnek, E. M. Wright, and J. V. Moloney, *Opt. Lett.* **23**, 382 (1998).  
 [4] M. Kolesik, E. M. Wright, and J. V. Moloney, *Phys. Rev. Lett.* **92**, 253901 (2004).  
 [5] N. Aközbek, C. M. Bowden, A. Talebpour, and S. L. Chin, *Phys. Rev. E* **61**, 4540 (2000).  
 [6] N. Aközbek, M. Scalora, C. M. Bowden, and S. L. Chin, *Opt. Commun.* **191**, 353 (2001).  
 [7] A. Couairon, *Phys. Rev. A* **68**, 015801 (2003).  
 [8] A. Couairon *et al.*, *J. Opt. Soc. Am. B* **19**, 1117 (2002).  
 [9] L. Bergé *et al.*, *Phys. Rev. Lett.* **92**, 225002 (2004).  
 [10] A. M. Perelomov, V. S. Popov, and M. V. Terent'ev, *Sov. Phys. JETP* **23**, 924 (1966). See also L. V. Keldysh, *ibid.* **20**, 1307 (1965); M. V. Ammosov, N. B. Delone, and V. P. Krainov, *ibid.* **64**, 1191 (1986).  
 [11] L. Bergé and A. Couairon, *Phys. Plasmas* **7**, 210 (2000).  
 [12] P. Sprangle, J. R. Peñano, and B. Hafizi, *Phys. Rev. E* **66**, 046418 (2002).  
 [13] G. P. Agrawal, *Nonlinear Fiber Optics*, 3rd ed. (Academic, New York, 2001).  
 [14] L. Bergé, Cl. Gouédard, J. Schjødt-Eriksen, and H. Ward, *Physica D* **176**, 181 (2003).